

Evaluation of the Simulation of Arctic and Antarctic Sea Ice Coverages
by Eleven Major Global Climate Models

Claire L. Parkinson¹, Konstantin Y. Vinnikov², and Donald J. Cavalieri¹

¹NASA Goddard Space Flight Center, Greenbelt, MD 20771

²University of Maryland, College Park, MD 20742

Significant Findings

Comparison of polar sea ice results from 11 major global climate models and satellite-derived observations for 1979-2004 reveals the following:

- Each of the models is simulating seasonal cycles that are phased at least approximately correctly in both hemispheres.
- Each of the models is simulating various key aspects of the ice cover distributions, such as winter ice not only throughout the central Arctic basin but also throughout Hudson Bay, despite its relatively low latitudes.
- Each of the models properly simulates a lack of winter ice to the west of Norway, although most do not simulate the observed absence of ice immediately north of Norway, suggesting a partial but under simulation of the North Atlantic Current.
- The German ECHAM5, Canadian CGCM3, and Japanese MIROC3 models do an excellent job at simulating the annual cycle of ice extents in the Northern Hemisphere.
- The Australian CSIRO Mk3 model does an excellent job at simulating the annual cycle of ice extents in the Southern Hemisphere, while the UK HadGEM1 and Canadian CGCM3 models simulate too much ice and the Japanese MIROC3, Norwegian BCCR BCM2, US GISS ER, US GFDL CM2.1, and especially the French IPSL CM4 models simulate too little ice in the Southern Hemisphere.
- The Canadian CGCM3, Japanese MIROC3, and French IPSL CM4 models do noticeably better in simulating the Northern Hemisphere ice extents than the Southern Hemisphere ice extents.
- The Australian CSIRO Mk3 model does noticeably better in simulating the Southern Hemisphere ice extents than the Northern Hemisphere ice extents.
- Each of the models simulates monthly average Northern Hemisphere ice extents to within $\pm 5.1 \times 10^6$ km² of the observed ice extent throughout the year.
- Each of the models except the French IPSL CM4 simulates monthly average Southern Hemisphere ice extents to within $\pm 6.3 \times 10^6$ km² of the observed ice extent throughout the year.
- The spread in monthly averaged ice extents amongst the 11 model simulations is greater in the Southern Hemisphere than in the Northern Hemisphere and greatest in the Southern Hemisphere winter and spring.

paper for submission to the *Journal of Geophysical Research*, November 2005

Corresponding author: Claire L. Parkinson (claire.l.parkinson@nasa.gov; 301-614-5715).

Evaluation of the Simulation of Arctic and Antarctic Sea Ice Coverages
by Eleven Major Global Climate Models

Claire L. Parkinson¹, Konstantin Y. Vinnikov², and Donald J. Cavalieri¹

¹Cryospheric Sciences Branch, NASA Goddard Space Flight Center, Greenbelt, MD 20771

²Department of Meteorology, University of Maryland, College Park, MD 20742

Index terms: 0750 Sea ice, 0700 Cryosphere, 0798 Modeling, 9310 Antarctica, 9315 Arctic region.

Corresponding author: Claire L. Parkinson, Code 614.1, NASA Goddard Space Flight Center, Greenbelt, MD 20771, email: claire.l.parkinson@nasa.gov, phone: 301-614-5715.

Abstract

Comparison of polar sea ice results from 11 major global climate models and satellite-derived observations for 1979-2004 reveals that each of the models is simulating seasonal cycles that are phased at least approximately correctly in both hemispheres. Each is also simulating various key aspects of the observed ice cover distributions, such as winter ice not only throughout the central Arctic basin but also throughout Hudson Bay, despite its relatively low latitudes. However, some of the models simulate too much ice, others too little ice (in some cases varying depending on hemisphere and/or season), and some match the observations better in one season versus another. Several models do noticeably better in the Northern Hemisphere than in the Southern Hemisphere, and one does noticeably better in the Southern Hemisphere. In the Northern Hemisphere all simulate monthly average ice extents to within $\pm 5.1 \times 10^6 \text{ km}^2$ of the observed ice extent throughout the year; and in the Southern Hemisphere all except one simulate the monthly averages to within $\pm 6.3 \times 10^6 \text{ km}^2$ of the observed values. All the models properly simulate a lack of winter ice to the west of Norway; however, most do not obtain as much absence of ice immediately north of Norway as the observations show, suggesting an under simulation of the North Atlantic Current. The spread in monthly averaged ice extents amongst the 11 model simulations is greater in the Southern Hemisphere than in the Northern Hemisphere and greatest in the Southern Hemisphere winter and spring.

1. Introduction

Considerable attention has been given to the difficulties of models in the simulation of the polar regions [e.g., *Proshutinsky et al.*, 2001; *Walsh et al.*, 2002]. These regions (Figure 1) have the complication of having a variable, ever-changing sea ice cover spreading over much of the ocean area. This ice cover restricts exchanges of heat, mass, and momentum between the ocean and atmosphere, strongly reflects incoming solar radiation, provides a net transport of relatively fresh and cold water equatorward, and affects the salinity and density structure of the underlying ocean [e.g., *Gordon and Taylor*, 1975; *Aagaard and Carmack*, 1989; *Barry et al.*, 1993; *Parkinson*, 2004]. Because of the strong coupling between sea ice and the rest of the climate system, errors in the simulation of the sea ice cover will be propagated to errors in the simulated atmosphere and ocean as well.

In this paper we present sea ice results from 11 major global climate models (GCMs) in both hemispheres and compare these results with observed sea ice coverages derived from satellite passive-microwave data, providing a sense of how well current GCMs are doing in the simulation of the polar sea ice covers. Results compared are the sea ice distributions in March and September and the monthly average sea ice extents throughout the annual cycle, in each case averaged for the 26-year period 1979-2004.

2. Data Sources

We obtained simulation results from the following web site of the Intergovernmental Panel on Climate Change (IPCC): <https://esg.llnl.gov:8443/home/publicHomePage.do>. These results have been provided by the respective modeling groups for the ongoing evaluations for the IPCC Fourth Assessment Report, updating the earlier IPCC Third

Assessment Report [Houghton *et al.*, 2001]. We selected all models with available output files for both sea ice concentration and sea ice thickness, although used only one run, “run1”, for each of the models. These models are listed and briefly described in the next section. In each case we used the twentieth century simulation (20C3M) run 1 for the years 1979 through the end of the 20C3M run 1 (i.e., through 1999 or 2000, depending on the model) and its continuation, run 1 of “future climate simulations: scenario SRES A2”, for the remaining years through 2004.

The observational data, used to compare with the modeled results, come from the data of the Scanning Multichannel Microwave Radiometer (SMMR) on the Nimbus 7 satellite and the Special Sensor Microwave Imagers (SSMIs) on the Defense Meteorological Satellite Program (DMSP) F8, F11, and F13 satellites. Details on the satellite data sets, their coregistration, and their use in Arctic and Antarctic sea ice studies can be found in *Cavalieri et al.* [1999], *Parkinson et al.* [1999], and *Zwally et al.* [2002]. The SMMR data were collected on an every-other-day basis for most of the period November 1978 – August 1987, and the SSMI data have been collected on a daily basis for most of the period since the June 1987 launch of the first SSMI. In this paper, we use the SMMR data for January 1979 – August 1987 and the SSMI data for August 1987 – December 2004.

As in *Parkinson et al.* [1999], *Zwally et al.* [2002], and elsewhere, ice extent is calculated from the satellite data as the sum of the areas of all grid cells with ice concentration (percent areal coverage of ice) of 15% or greater. For the models, we used the criteria that the ice concentration must be at least 15% and the ice thickness must be at least 6 cm, as the satellite imagery does not sense the extremely thin ice.

3. The Models

The 11 GCMs employed in this study and their IPCC identifications (IDs) are:

1. The United Kingdom Met Office (UKMO) Hadley Centre Coupled Model 3 (HadCM3) from the Hadley Centre for Climate Prediction and Research at the UKMO, United Kingdom. This is a coupled atmosphere-ocean GCM with 19 vertical layers and a horizontal resolution of 2.5° latitude x 3.75° longitude in the atmosphere and 20 vertical layers and a horizontal resolution of 1.25° latitude x 1.25° longitude in the ocean. The sea ice formulation includes ice thermodynamic calculations, one ice layer in the vertical, and ice advection strictly with the ocean current. The ice calculations are divided between the atmosphere and ocean model components. The model shows little drift in surface climate in a control run of over a thousand years, despite not using flux adjustments. The model is described in *Gordon et al. [2000]* and *Pope et al. [2000]*. IPCC ID: UKMO-HadCM3.

2. The United Kingdom Met Office (UKMO) Hadley Centre Global Environmental Model version 1 (HadGEM1) from the Hadley Centre for Climate Prediction and Research at the UKMO, United Kingdom. This is a new coupled climate model developed at the Hadley Centre starting in 2000 as an eventual replacement for the HadCM3 model, with advances in particular in the sea ice and atmosphere components. It has 38 vertical layers and a horizontal resolution of 1.25° latitude x 1.875° longitude in the atmosphere, while in the ocean it has 40 vertical layers, a zonal resolution of 1° , and a meridional resolution that is 1° poleward of 30° and smoothly varies from 0.333° at the equator to 1° at 30° latitude. The sea ice formulation includes ice thermodynamics, ice dynamics, one ice layer in the vertical, and multiple ice thicknesses allowed in a grid cell. The sea ice calculations in the HadGEM1 model, like those in the HadCM3 model, are divided between the atmosphere

and ocean components. The HadGEM1 model is described in *Johns et al.* [2005]. IPCC ID: UKMO-HadGEM1.

3. The European Centre for Medium-Range Weather Forecasts (ECMWF) Hamburg Model version 5 (ECHAM5), from the Max Planck Institute for Meteorology (MPI), Hamburg, Germany. This fifth generation ECHAM model uses a spectral, semi-implicit formulation for the atmosphere, with 31 vertical layers, and an ocean with 40 vertical layers and 1.5° latitude x 1.5° longitude horizontal resolution. The sea ice formulation includes ice dynamics, ice thermodynamics, one ice layer in the vertical plus an overlying snow layer, one ice thickness category, and 1.5° latitude x 1.5° longitude horizontal resolution. The sea ice calculations are done within the ocean component. The atmosphere component is described in *Roeckner et al.* [2003], and the ocean component is described in *Marsland et al.* [2003]. IPCC ID: ECHAM5/MPI-OM.

4. The Canadian Centre for Climate Modelling & Analysis (CCCma) Third Generation Coupled Global Climate Model (CGCM3) from the CCCma, Environment Canada, University of Victoria, Canada. The third generation model has a substantially updated atmospheric component over the CGCM2, and details can be found at <http://www.cccma.bc.ec.gc.ca/models/cgcm3.shtml>. Results from two versions of the model, T47 and T63, were provided to the IPCC. We used the results from the lower-resolution T47 version, with 31 vertical layers and a spatial resolution of approximately 3.75° latitude x 3.75° longitude in the atmosphere and 29 vertical layers and a spatial resolution of approximately 1.85° latitude x 1.85° longitude in the ocean. The sea ice formulation includes ice thermodynamics, ice dynamics, and a single ice thickness per grid cell. Details on the model's ocean component can be found in *Kim et al.* [2002]. IPCC ID: CGCM3.1.

5. The Commonwealth Scientific and Industrial Research Organization (CSIRO) Mark 3.0 model from CSIRO, Australia. This is a vintage 2001 model with 18 vertical layers and a horizontal resolution of approximately 1.875° latitude x 1.875° longitude in the atmosphere/land/ice component and 31 vertical layers and a horizontal resolution of approximately 1.875° longitude x 0.84° latitude in the ocean component. The sea ice formulation includes ice thermodynamics, ice dynamics, one or two ice layers in the vertical depending on ice thickness, and an overlying snow layer. The sea ice calculations are done as part of the atmosphere component, with the same spatial resolution. The CSIRO Mark 3.0 model is described in detail in *Gordon et al.* [2002]. IPCC ID: CSIRO-Mk3.0.

6. The medium resolution version of the Model for Interdisciplinary Research on Climate (MIROC), version 3.2, from the Center for Climate System Research (CCSR) at the University of Tokyo, the Japan National Institute for Environmental Studies (NIES), and the Frontier Research Center for Global Change (FRCGC), Japan. The atmospheric component in the medium resolution framework has 20 vertical layers and a horizontal resolution approximately equivalent to 2.8° latitude x 2.8° longitude, while the ocean component has 43 vertical layers, a zonal resolution of approximately 1.4° , and a meridional resolution varying from approximately 0.56° at low latitudes to approximately 1.4° at high latitudes. The sea ice formulation includes ice thermodynamics, ice dynamics, one ice layer in the vertical and an overlying snow layer, two ice thickness categories allowed in a grid cell, and a spatial resolution of 1.4° in both latitude and longitude. The MIROC model is described in *Hasumi and Emori* [2004]. IPCC ID: MIROC3.2 (medres).

7. The Bjerknes Centre for Climate Research (BCCR) Bergen Climate Model (BCM) version 2, from the BCCR at the University of Bergen, Norway. The atmospheric

component has 31 vertical layers and a linear reduced Gaussian grid [*Hortal and Simmonds, 1991*] equivalent to approximately 2.8° latitude x 2.8° longitude spatial resolution. The ocean component has 35 vertical layers, 1.5° zonal resolution, and meridional resolution varying from 0.5° to 1.5° depending on latitude. The sea ice formulation includes ice thermodynamics, ice dynamics, one ice layer in the vertical overlain by a snow layer, and a single ice thickness per grid cell. The ice calculations are done within the model's ocean component, with four ice grid cells within each ocean grid cell. Additional information can be found at http://www-pcmdi.llnl.gov/ipcc/model_documentation/BCCR_BCM2.0.pdf. IPCC ID: BCCR-BCM2.0.

8. The Goddard Institute for Space Studies (GISS) model ER, from GISS, National Aeronautics and Space Administration (NASA), United States. The GISS Model E is an atmospheric GCM described in detail in *Schmidt et al. [2005]*. "E" here has no meaning beyond being the next letter in the alphabet in a list of GISS models. "R" refers to the coupling of Model E with an ocean model whose development was led by G. Russell. Model ER has 20 vertical layers in the atmosphere, 13 vertical layers in the ocean, and a spatial resolution of 4° latitude x 5° longitude for both the atmosphere and ocean. The sea ice formulation includes ice thermodynamics, ice dynamics, four ice layers in the vertical overlain by one snow layer, and one ice thickness category per grid cell. The ice calculations are incorporated as part of the model's atmosphere component, with the same resolution. Additional information can be found in *Schmidt et al. [2005]* and *Russell et al. [2000]*. IPCC ID: GISS ER.

9. The Institut Pierre Simon Laplace (IPSL) coupled model (CM) 4 from IPSL, France. The atmosphere component has 19 vertical layers and a spatial resolution of 2.5° latitude x

3.75° longitude. It is described in *Hourdin et al.* [2005]. The ocean component has 31 vertical layers, a spatial resolution of 2° latitude x 2° longitude, and a tri-polar grid, with one pole at the South Pole, one over Canada, and one over Siberia, avoiding a singularity at the North Pole. The sea ice formulation includes ice thermodynamics, ice dynamics, two ice layers in the vertical overlain by a snow layer, and a spatial resolution as in the ocean model, 2° latitude x 2° longitude. Further details can be found in *Marti et al.* [2005]. IPCC ID: IPSL-CM4.

10. The Institute of Numerical Mathematics (INM) CM3.0 model, from INM, Russian Academy of Science, Russia. The atmosphere component has 21 vertical layers and a spatial resolution of 4° latitude x 5° longitude. The ocean component has 33 vertical layers, a rigid lid, and a spatial resolution of 2° latitude x 2.5° longitude. Both the atmosphere and ocean components have sigma vertical coordinates. The sea ice formulation is strictly thermodynamic, with one layer in the vertical, one thickness category, and the same spatial resolution as for the ocean component. Further details can be found in *Diansky et al.* [2002] and *Diansky and Volodin* [2002]. IPCC ID: INM-CM3.0.

11. The Geophysical Fluid Dynamics Laboratory (GFDL) coupled model (CM) 2.1, from GFDL, National Oceanic and Atmospheric Administration (NOAA), United States. The atmosphere component has 24 vertical layers and a horizontal resolution of 2° latitude x 2.5° longitude, with a hybrid sigma-pressure vertical coordinate. The ocean component has 50 vertical layers and 1° latitude x 1° longitude horizontal resolution at mid and high latitudes, with enhanced resolution in the tropics, down to 0.333° at the equator, and with poles over North America and Eurasia to avoid complications at the geographic North Pole. The sea ice formulation includes ice thermodynamics, ice dynamics, two ice layers overlain

by one snow layer, five thickness categories allowed in a grid cell, and the same horizontal grid as used in the ocean component. The CM2.1 model does not employ flux adjustments. Additional details about the GFDL CM2.1 model can be found in *Zhang and Delworth [2005]* and *Delworth et al. [2005]*. IPCC ID: GFDL-CM2.1.

4. Results

Figure 2 presents summer and winter sea ice distributions from the satellite observations (Figure 2A) and from each of the 11 models (Figures 2B-2L), averaged over the 26 years 1979-2004. Results are presented for September and March of each hemisphere. In the Northern Hemisphere, September is typically the month of minimum ice coverage and March is typically the month of maximum ice coverage. In the Southern Hemisphere, September is often the month of maximum ice coverage, although maximum ice coverage can alternatively occur in either August or October. February is generally the month of minimum ice coverage in the Southern Hemisphere, with the ice cover growing somewhat in March, at the end of summer and start of autumn.

Figure 3 presents the full annual cycle of monthly average ice extents for both hemispheres, again averaged for 1979-2004, first from the observations (Figure 3A) and then from simulations of the 11 GCMs (Figures 3B-3L). The observations show the 26-year-average Arctic sea ice cover reaching a minimum extent of $6.8 \times 10^6 \text{ km}^2$ in September and rising to a maximum extent of $15.3 \times 10^6 \text{ km}^2$ in March and the 26-year-average Antarctic sea ice cover reaching a minimum extent of $3.0 \times 10^6 \text{ km}^2$ in February and rising to a maximum extent of $18.2 \times 10^6 \text{ km}^2$ in September (Figure 3A).

Although each model properly simulates out-of-phase seasonal cycles in the two hemispheres, with low ice amounts at the end of the respective summers and high ice amounts at the end of the respective winters, the phasing and especially the amplitudes of the cycles vary noticeably among the models, as does the closeness of the match of the simulated ice covers versus the observations. The UK HadCM3 model simulates most aspects of the seasonal cycle of ice extents quite well, although maximum simulated ice extents in both hemispheres are higher than in the observations and are delayed by about a month versus the observations (Figure 3B). The March map shows that the excess Northern Hemisphere winter ice is largely in the Greenland and Barents Seas, suggesting an under simulation of the Gulf Stream and North Atlantic Current. The Southern Hemisphere HadCM3 map shows too little late winter ice in the vicinity of the Greenwich meridian but too much ice from 70°E eastward to 100°W and too little summertime ice in the western hemisphere (Figure 2B).

The UK HadGEM1 model has greater ice extents than the observations throughout the year, with the excess versus the observations being particularly great in the Southern Hemisphere winter. This model simulates the correct timing of minimum ice extent in both hemispheres and of maximum ice extent in the Northern Hemisphere, while simulating maximum Southern Hemisphere ice coverage as occurring in October, one month delayed versus the observations (Figure 3C). The Northern Hemisphere March map shows a very good match (although with somewhat too much ice) with the observed pattern of ice coverage throughout the entire North Atlantic vicinity (Labrador Sea, Davis Strait, Greenland Sea, Barents Sea), although has too much ice on the Pacific side, in both the Bering and Okhotsk seas. Summertime ice is too extensive in Baffin Bay and immediately

north of western Canada and Alaska, although is somewhat less extensive than the observations in the Greenland Sea and just north of the Barents and Kara seas. It has successfully simulated more summer ice than HadCM3. In the Southern Hemisphere, the geographic pattern of the wintertime ice cover is improved over that of the HadCM3 model, although the ice cover is excessive around much of the continent. The simulation of the pattern of summertime ice has also improved, especially in the western Weddell Sea, although the ice amount is excessive, with the excess ice coming largely in the eastern Weddell Sea and the eastern hemisphere (Figure 2C).

The German ECHAM5 model properly simulates the timing of maximum and minimum ice coverage and for all except the summer months, even simulates the correct magnitudes of the ice extents in the Northern Hemisphere. The extent magnitudes are also close to the observed values in the Southern Hemisphere throughout the decay period, while being too low during the growth period (Figure 3D). The distribution of simulated March ice cover in the Northern Hemisphere is excellent, while the simulated September ice is somewhat too great around the entire periphery of the ice cover, inappropriately spreading southward to the western Canadian, Alaskan, and Russian coasts, as well as being excessive in the Greenland Sea and the northern Barents and Kara Seas (Figure 2D), although the entire excess is less than 30% (Figure 3D). In the Southern Hemisphere, the simulated September, late-winter ice is too extensive in the western Weddell Sea, especially near 30°W, and in the Amundsen Sea, but is not extensive enough in the eastern Weddell Sea and around much of East Antarctica (Figure 2D). The excesses and underestimates balance each other so well that the ice extent for September is within 2% of the observed extent (Figure 3D). The simulated March Southern Hemisphere ice distributions are reasonable around much of the

continent although with too little ice in the Amundsen and eastern Ross Seas and too much ice in the western Ross Sea (Figure 2D).

The Canadian CGCM3 model simulates correct maximum and minimum timings in both hemispheres and does an excellent job in simulating the annual cycle of Northern Hemisphere ice extent magnitudes although simulates considerably too much Southern Hemisphere ice, especially in the winter (Figure 3E). Spatially, the coarse resolution of the model grid prohibits a simulation of the details of the ice edge, but to the level allowed by the resolution, the model does very well in simulating the winter ice in the Sea of Okhotsk and Hudson Bay and the absence of ice west of Norway. Excessive ice coverage appears in the Labrador Sea and immediately north of Iceland, while too little ice appears along the southeast coast of Greenland. In September, somewhat excessive ice coverage appears around most of the periphery of the central Arctic Basin and too little ice appears to the east of Greenland, although in many areas the differences from the observations can be accounted for by the coarse model resolution. In the Southern Hemisphere, excess wintertime ice appears around most of the continent and excess summertime ice appears especially in the eastern Weddell Sea (Figure 2E).

In contrast to the Canadian CGCM3 model, with its superior simulation of the Northern Hemisphere ice cover, the Australian CSIRO Mk3 model does a superior job in the simulation of the Southern Hemisphere ice. The CSIRO Mk3 Southern Hemisphere simulation has ice extents matching the observed values almost precisely for much of the growth period, although has a month delay in the timing of minimum and maximum ice coverage and somewhat too much ice in the ice decay period. The Northern Hemisphere simulation has too much ice throughout the year but especially in summer, with a resulting

under simulation of the amplitude of the annual cycle (Figure 3F). Spatially, the significant excess of ice in the Northern Hemisphere summer appears most prominently in the Kara and Barents Seas, although is also apparent in the existence of ice in northern Baffin Bay and the extension of the central Arctic ice to the North American, Asian, and European coasts. The excessive ice in both summer and winter seasons in the Barents Sea suggests an under simulation of the Gulf Stream and North Atlantic Current. Wintertime ice in the Greenland Sea is also excessive, while that in the Bering Sea is underrepresented (Figure 2F). Simulation of the Southern Hemisphere ice distributions is considerably better, although with too much late-summer ice in the western Ross and eastern Weddell Seas and too little summer ice around much of East Antarctica (Figure 2F).

Like the Canadian model, the Japanese MIROC3 model does a superior job in simulating the Northern Hemisphere ice versus the Southern Hemisphere ice. The MIROC3 results have the timing of maximum and minimum ice extent in the Southern Hemisphere correct and a quite reasonable amplitude for the annual cycle but have too little ice throughout the year. The MIROC3 Northern Hemisphere ice extents are much closer in magnitude to the observations, with the difference between simulated and observed monthly average extents being greatest in September, and even then the excess in simulated ice extent is only 22%. This excess is due in part to the early simulated ending of the decay period, minimum ice extent coming in August rather than September (Figure 3G). Spatially, the Southern Hemisphere September modeled results have too little ice in the Amundsen, eastern Ross, and especially the eastern Weddell Sea, with an interesting capturing of a pattern of ice in the western Weddell Sea reflective of the clockwise Weddell Gyre that is sometimes seen in the observations, although in the December-May time frame rather than

in September. The March simulation results have too little ice in the western Weddell Sea and in the southern Bellingshausen and Amundsen Seas and eastern Ross Sea, with too much ice in the western Ross Sea (Figure 2G). In the Northern Hemisphere, the excess Northern Hemisphere summer ice simulated by the model is predominantly immediately north of Eurasia and in northern Baffin Bay, whereas most of the small amount of excess wintertime ice is in the Barents Sea and eastern Sea of Okhotsk, suggestive of a weak North Atlantic Current and a weak eastern Okhotsk current (Figure 2G).

The Norwegian BCCR BCM2 model simulates annual cycles with amplitudes matching well with the observations in both hemispheres. There is, however, too little ice simulated in the Antarctic and too much ice in the Arctic, with the timing of minimum monthly average ice extent correct in both cases but the timing of maximum ice extent delayed by one month in the Southern Hemisphere (Figure 3H). Spatially, the excess Northern Hemisphere wintertime ice is apparent in the Bering Sea, Sea of Okhotsk, Barents Sea, and north of Iceland, with too little ice simulated in the Labrador Sea and along the southeastern coast of Greenland. In late summer, most of the excess ice is in the Kara and Barents Seas and immediately north of Russia. In the Southern Hemisphere, the region most deficient in simulated September (winter) ice is the eastern Weddell Sea and the region most deficient in simulated March (summer) ice is the Amundsen and eastern Ross Seas. In contrast, the western Ross Sea contains a slight excess of simulated ice and the Weddell Sea has a realistic simulated ice cover, with substantial ice in the western portion of the sea and no ice in the eastern portion (Figure 2H).

The U.S. GISS ER model does a good job at simulating the amplitude of the seasonal cycle in the Southern Hemisphere, although with too little ice through much of the year and

a one-month delay, until October, in the reaching of maximum ice coverage. In the Northern Hemisphere, somewhat too much ice is simulated throughout the year, especially in summer, with the result that the amplitude of the annual cycle is under simulated (Figure 3I). The coarse resolution of the model grid is apparent in the maps and hinders simulation of the details of the ice edge. In both the March and September Northern Hemisphere results, the excess ice is particularly apparent in the Barents Sea and the northern Greenland Sea. The simulation of ice throughout the Barents Sea even in summertime suggests a strong under simulation of the northward water flow from the North Atlantic Current. The under simulation of Southern Hemisphere ice is apparent in the lack of ice along most of the East Antarctic coast from about 75°E to about 160°E in both March and September, likely in part because of the coarse model resolution. In March there is also a notable absence of ice in the Bellingshausen and Amundsen Seas and too little ice in the western Weddell Sea. In wintertime, there is too much ice in the Amundsen Sea but appropriate ice distributions, to the resolution of the model, in the Weddell Sea and east to about 75°E and in much of the Ross and Bellingshausen Seas (Figure 2I).

The French IPSL CM4 model does a much better job at simulating the Northern than the Southern Hemisphere ice cover, although fails to simulate enough ice in either hemisphere and has the timings of minimum ice coverage about one month late. The Southern Hemisphere simulation in particular has too little ice, with the ice throughout the year being less than 37% of the observed values and in all months except September and October being less than 30% of the observed values (Figure 3J). Spatially, the September Southern Hemisphere winter ice cover is appropriate in the western Weddell Sea and off East Antarctica at about 140°E but not extensive enough around the rest of the continent.

The simulated March ice cover is well under the observed amounts but does properly show that the greatest amount of late summer ice is in the western Weddell Sea. In contrast, the Northern Hemisphere simulated ice distributions are much closer to the observations, especially in September, when the simulated distribution is excellent, having an appropriately positioned tongue of ice along the east coast of Greenland, an appropriate simulation of ice along the north coast of Greenland and the northernmost Canadian islands, and an appropriate retreat of the ice from the Alaskan and much of the Russian coast. The simulated Northern Hemisphere March ice cover has too little ice in the Bering and Okhotsk Seas but an appropriate ice distribution in Davis Strait and the Labrador Sea. The IPSL CM4 model does much better than many models in simulating the warming influence of the North Atlantic Current as far north as north of Norway and the extension of the tongue of ice along the east coast of Greenland almost to the southern tip of the island. Although there is somewhat too much ice in this North Atlantic region, overall the pattern of wintertime ice distributions in this region is excellent (Figure 2J).

The Russian INM CM3 model does well in simulating the amplitude of the Northern Hemisphere annual cycle and the timing of minimum ice extent, although with too little ice in each month. In the Southern Hemisphere it does well in simulating ice extents in spring and summer but simulates too great and rapid an expansion of the ice cover in autumn and early winter, with a peak ice extent of $21 \times 10^6 \text{ km}^2$ in August, a month prior to the observed monthly average peak of $18.2 \times 10^6 \text{ km}^2$ in September (Figure 3K). Spatially, there is a proper simulation of the March wintertime ice covering the Arctic Basin, the Kara Sea, and Hudson Bay, but too little winter ice in Baffin Bay, the Labrador Sea, along the east coast of Greenland and in the Sea of Okhotsk, canceled in part by too much winter ice in the western

Bering Sea. Simulated September Northern Hemisphere ice is properly centered a little to the Bering Strait side of the North Pole but is not as extensive as the observed ice cover. In the Southern Hemisphere, the pattern of March late-summer ice is simulated quite well, although with too much ice in the Ross Sea. The simulated pattern of September late-winter ice has considerably too extensive an ice cover in the Bellingshausen and Amundsen Seas and too little ice in the eastern Weddell Sea (Figure 2K).

The U.S. GFDL CM2.1 model simulates the amplitude of the seasonal cycle in the Southern Hemisphere quite well, although with too little ice throughout the year. It also properly simulates the timing of maximum and minimum ice extents in both hemispheres. In the Northern Hemisphere, the GFDL simulation obtains too much ice in the winter and too little ice in the summer, resulting in an amplified annual cycle (Figure 3L). The GFDL results have the Southern Hemisphere ice cover reducing to only $0.03 \times 10^6 \text{ km}^2$ in February (versus the observed $3.03 \times 10^6 \text{ km}^2$) (Figure 3L), with a small amount of ice beginning to form at coastal locations in March (Figure 2L), well under the observed March ice coverage (Figure 2A). The September distribution of the Southern Hemisphere ice is excellent around most of the Antarctic continent except in the Weddell Sea, where there is too little ice (Figure 2L). The Northern Hemisphere March simulated ice distribution shows the excess wintertime ice to be most apparent on the Pacific side, in the Bering Sea and Sea of Okhotsk, with some excess ice also in the eastern Barents Sea and the Greenland Sea. The wintertime ice distributions in the Davis Strait and Labrador Sea regions are excellent. The simulated Northern Hemisphere summertime ice is not nearly extensive enough but otherwise is well distributed (Figure 2L).

All 11 models properly simulate that Hudson Bay, despite its low latitudes, is covered with ice in March, and all except one of the models properly simulate that this ice has totally retreated from the bay in September (Figure 2). They also all properly simulate that there is no ice from the west of Norway to the Greenwich meridian along most of the Norwegian coast even in March and that wintertime ice fully covers the Arctic Basin (to at least 15% ice coverage in each grid cell). In the Southern Hemisphere, 9 of the 11 models properly simulate wintertime ice surrounding the entire continent of Antarctica (Figure 2).

5. Summary and Discussion

Sea ice results from 11 major GCM simulations have been compared with satellite observed sea ice extents averaged by month for the period 1979-2004. Each model appropriately simulates a seasonal cycle with greater ice extent in the winter than the summer of each hemisphere, and each model appropriately simulates certain basic observed features, such as an ice-covered Hudson Bay in winter, despite its relatively low latitudes, and an ice-free span from Iceland to Norway, despite its higher latitudes. However, some models simulate too much ice, others too little ice (in some cases varying depending on hemisphere and/or season), and some models match the observations noticeably better in either the growth or decay season. Similarly, some models match the observations better in the Northern Hemisphere (e.g., the CGCM3 and the MIROC3) and others match the observations better in the Southern Hemisphere (e.g., the CSIRO Mk3).

When the annual cycles of the ice extent differences between the simulated and observed results for each of the 11 models are plotted together (Figure 4), it becomes clear that, overall, the modeled annual cycles are more similar among themselves and closer to the

observations in the Northern Hemisphere than in the Southern Hemisphere. In the Northern Hemisphere, all monthly average modeled ice extents lie within $\pm 5.1 \times 10^6 \text{ km}^2$ of the observed ice extent throughout the year, and the spread amongst the models is greatest in the summer and autumn months, especially August and September (Figure 4A). In the Southern Hemisphere, there is a noticeably larger spread amongst the model results, although still all models except one have simulated monthly average ice extents that consistently lie within $\pm 6.3 \times 10^6 \text{ km}^2$ of the observed ice extents (Figure 4B). In contrast to the Northern Hemisphere, in the Southern Hemisphere the greatest spread amongst the model results occurs during the winter and spring months (Figure 4). When the results from all 11 models are averaged, the simulated average monthly ice extents are all greater than the observed in the Northern Hemisphere (by amounts ranging from $0.04 \times 10^6 \text{ km}^2$ in December to $1.2 \times 10^6 \text{ km}^2$ in May) and are all less than the observed in the Southern Hemisphere (by amounts ranging from $0.3 \times 10^6 \text{ km}^2$ in February to $1.9 \times 10^6 \text{ km}^2$ in May). In fact, despite the variety of problems with the individual simulations, the ensemble average of the 11 model simulations does reasonably well in simulating the annual cycle of sea ice extents in each hemisphere (Figure 5). Percentage-wise, the ensemble Northern Hemisphere monthly averages are all greater than the observations by values ranging from 0.3% in December to 13.9% in September, and the ensemble Southern Hemisphere monthly averages are all less than the observations by values ranging from 2.6% in October to 26.0% in April.

These results essentially show a snapshot of how well the 11 examined GCMs are doing in the simulation of the polar sea ice covers as of the submission of the modeling results for the upcoming IPCC Fourth Assessment Report. All of the models simulate some aspects of the sea ice covers well, but some of the models have severe deficiencies in other aspects, as

detailed in the previous section and in Figures 2-3. However, model development continues in each of the modeling groups, and hence some of the shortcomings of the model simulations are likely to be improved upon in subsequent versions of the models. By soliciting simulation results from modeling groups from around the world and making them available to interested scientists, the IPCC effort enables comparative studies, such as the one in this paper, that can identify strengths and weaknesses of the results versus the observations and thereby, ideally, can help both in the continuing improvement of the models and in the interpretation of the modeled results.

Acknowledgments

The authors greatly appreciate the 11 modeling groups for making their simulation results available and the Program for Climate Model Diagnostics and Intercomparison at Lawrence Livermore National Laboratory for compiling and providing internet access to these results. We also greatly appreciate Nick DiGirolamo for his help in the processing of the satellite data and in the generation of two of the figures. This work was supported by the Cryospheric Sciences Program at NASA Headquarters.

References

- Aagaard, K., and E. C. Carmack (1989), The role of sea ice and other fresh water in the Arctic circulation, *J. Geophys. Res.*, *94*(C10), 14,485-14,498.
- Barry, R. G., M. C. Serreze, J. A. Maslanik, and R. H. Preller (1993), The Arctic sea ice-climate system: Observations and modeling, *Rev. Geophys.*, *31*(4), 397-422.
- Cavalieri, D. J., C. L. Parkinson, P. Gloersen, J. C. Comiso, and H. J. Zwally (1999), Deriving long-term time series of sea ice cover from satellite passive-microwave multisensor data sets, *J. Geophys. Res.*, *104*(C7), 15,803-15,814.
- Delworth, T. L., A. J. Broccoli, A. Rosati, R. J. Stouffer, V. Balaji, J. A. Beesley, W. F. Cooke, K. W. Dixon, J. Dunne, K. A. Dunne, J. W. Durachta, K. L. Findell, P. Ginoux, A. Gnanadesikan, C. T. Gordon, S. M. Griffies, R. Gudgel, M. J. Harrison, I. M. Held, R. S. Hemler, L. W. Horowitz, S. A. Klein, T. R. Knutson, P. J. Kushner, A. R. Langenhorst, H.-C. Lee, S.-J. Lin, J. Lu, S. L. Malyshev, P. C. D. Milly, V. Ramaswamy, J. Russell, M. D. Schwarzkopf, E. Shevliakova, J. J. Sirutis, M. J. Spelman, W. F. Stern, M. Winton, A. T. Wittenberg, B. Wyman, F. Zeng, and R. Zhang (2005), GFDL's CM2 global coupled climate models – Part 1: Formulation and simulation characteristics, *J. Climate*, in press. (Preprint available at <http://nomads.gfdl.noaa.gov/CM2.X/references/>.)
- Diansky, N. A., A. V. Bagnò, and V. B. Zalesny (2002), Sigma model of global ocean circulation and its sensitivity to variations in wind stress, *Izv. Atmos. Ocean. Phys.*, *38*(5), 477-494.
- Diansky N. A., and E. M. Volodin (2002), Simulation of present-day climate with a coupled atmosphere-ocean general circulation model, *Izv. Atmos. Ocean. Phys.*, *38*(6), 732-747.

- Gordon, A. L., and H. W. Taylor (1975), Seasonal change of Antarctic sea ice cover, *Science*, *187*, 346-347.
- Gordon, C., C. Cooper, C. A. Senior, H. Banks, J. M. Gregory, T. C. Johns, J. F. B. Mitchell, and R. A. Wood (2000), The simulation of SST, sea ice extents and ocean heat transports in a version of the Hadley Centre coupled model without flux adjustments, *Climate Dyn.*, *16*, 147-168.
- Gordon, H. B., L. D. Rotstayn, J. L. McGregor, M. R. Dix, E. A. Kowalczyk, S. P. O'Farrell, L. J. Waterman, A. C. Hirst, S. G. Wilson, M. A. Collier, I. G. Watterson, and T. I. Elliott (2002), The CSIRO Mk3 Climate System Model, *CSIRO Atmospheric Research Technical Paper No. 60*, 130 pp., CSIRO Australia, Aspendale, Australia. (Electronic publication, available at http://www.dar.csiro.au/publications/gordon_2002a.pdf.)
- Hasumi, H., and S. Emori (Eds.) (2004), K-1 Coupled GCM (MIROC) Description, *K-1 Technical Report No. 1*, 34 pp., Center for Climate System Research, University of Tokyo, Tokyo. (Available at <http://www.ccsr.u-tokyo.ac.jp/kyosei/hasumi/MIROC/tech-repo.pdf>.)
- Hortal, A., and A. J. Simmons (1991), Use of reduced Gaussian grids in spectral models, *Mon. Wea. Rev.*, *119*, 1057-1074.
- Houghton, J. T., Y. Ding, D. J. Griggs, M. Noguer, P. J. van der Linden, X. Dai, K. Maskell, and C. A. Johnson (Eds.) (2001), *Climate Change 2001: The Scientific Basis. Contribution of Working Group I to the Third Assessment Report of the Intergovernmental Panel on Climate Change*, 881 pp., Cambridge Univ. Press, New York.

- Hourdin, F., I. Musat, S. Bony, P. Braconnot, F. Codron, J.-L. Dufresne, L. Fairhead, M.-A. Filiberti, P. Friedlingstein, J.-Y. Grandpeix, G. Krinner, P. LeVan, Z.-X. Li, and F. Lott (2005), The LMDZ4 general circulation model: Climate performance and sensitivity to parametrized physics with emphasis on tropical convection, *Climate Dyn.*, submitted.
- Johns, T., C. Durman, H. Banks, M. Roberts, A. McLaren, J. Ridley, C. Senior, K. Williams, A. Jones, A. Keen, G. Rickard, S. Cusack, M. Joshi, M. Ringer, B. Dong, H. Spencer, R. Hill, J. Gregory, A. Pardaens, J. Lowe, A. Bodas-Salcedo, S. Stark, and Y. Searl (2005), HadGEM1 – Model description and analysis of preliminary experiments for the IPCC Fourth Assessment Report, *Hadley Centre Technical Note 55*, 74 pp., Hadley Centre, Exeter, UK. (Available electronically at http://www.metoffice.com/research/hadleycentre/pubs/HCTN/HCTN_55.pdf; February 2005 update to an October 2004 document.)
- Kim, S.-J., G. M. Flato, G. J. Boer, and N. A. McFarlane (2002), A coupled climate model simulation of the Last Glacial Maximum, Part 1: Transient multi-decadal response, *Climate Dyn.*, *19*, 515-537.
- Marsland, S. J., H. Haak, J. H. Jungclauss, M. Latif, and F. Röske (2003), The Max Planck Institute global ocean/sea-ice model with orthogonal curvilinear coordinates, *Ocean Modelling*, *5*, 91-127.
- Marti, O., P. Braconnot, J. Bellier, R. Benshila, S. Bony, P. Brockmann, P. Cadulle, A. Caubel, S. Denvil, J. L. Dufresne, L. Fairhead, M.-A. Filiberti, T. Fichefet, P. Friedlingstein, J.-Y. Brandpeix, F. Hourdin, G. Krinner, C. Lévy, I. Musat, and C. Talandier (2005), The new IPSL climate system model: IPSL-CM4, 86 pp. Institut

Pierre Simon Laplace des Sciences de l'Environnement Global, Paris. (Available at <http://dods.ipsl.jussieu.fr/omamce/IPSLCM4/DocIPSLCM4/FILES/DocIPSLCM4.pdf>.)

Parkinson, C. L. (2004), Southern Ocean sea ice and its wider linkages: Insights revealed from models and observations, *Antarctic Science*, 16(4), 387-400, doi:10.1017/S0954102004002214.

Parkinson, C. L., D. J. Cavalieri, P. Gloersen, H. J. Zwally, and J. C. Comiso (1999), Arctic sea ice extents, areas, and trends, 1978-1996, *J. Geophys. Res.*, 104(C9), 20,837-20,856.

Pope, V. D., M. L. Gallani, P. R. Rowntree, and R. A. Stratton (2000), The impact of new physical parameterizations in the Hadley Centre climate model – HadAM3, *Climate Dyn.*, 16, 123-146.

Proshutinsky, A., M. Steele, J. Zhang, G. Holloway, N. Steiner, S. Hakkinen, D. Holland, R. Gerdes, C. Koeberle, M. Karcher, M. Johnson, W. Maslowski, W. Walczowski, W. Hibler, and J. Wang (2001), Multinational effort studies differences among Arctic Ocean models, *Eos*, 82(51), 637, 643-644.

Roeckner, E., G. Bäuml, L. Bonaventura, R. Brokopf, M. Esch, M. Giorgetta, S. Hagemann, I. Kirchner, L. Kornbluch, E. Manzini, A. Rhodin, U. Schlese, U. Schulzweida, and A. Tompkins (2003), The atmospheric general circulation model ECHAM5. Part I: Model description, *Max Planck Institute for Meteorology Report 349*, 127 pp., Max Planck Institute for Meteorology, Hamburg, Germany.

Russell, G. L., J. R. Miller, D. Rind, R. A. Ruedy, G. A. Schmidt, and S. Sheth (2000), Comparison of model and observed regional temperature changes during the past 40 years, *J. Geophys. Res.*, 105, 14,891-14,898.

- Schmidt, G. A. , R. Ruedy, J. E. Hansen, I. Aleinov, N. Bell, M. Bauer, S. Bauer, B. Cairns, V. Canuto, Y. Cheng, A. DelGenio, G. Faluvegi, A. D. Friend, T. M. Hall, Y. Hu, M. Kelley, N. Y. Kiang, D. Koch, A. A. Lacis, J. Lerner, K. K. Lo, R. L. Miller, L. Nazarenko, V. Oinas, Ja. Perlwitz, Ju. Perlwitz, D. Rind, A. Romanou, G. L. Russell, M. Sato, D. T. Shindell, P. H. Stone, S. Sun, N. Tausnev, D. Thresher, and M.-S. Yao (2005), Present day atmospheric simulations using GISS ModelE: Comparison to in-situ, satellite and reanalysis data, *J. Climate*, in press.
- Walsh, J. E., V. M. Kattsov, W. L. Chapman, V. Govorkova, and T. Pavlova (2002), Comparison of Arctic climate simulations by uncoupled and coupled global models, *J. Climate*, *15*, 1429-1446.
- Zhang, R., and T. L. Delworth (2005), Simulated tropical response to a substantial weakening of the Atlantic thermohaline circulation, *J. Climate*, *18*, 1853-1860.
- Zwally, H. J., J. C. Comiso, C. L. Parkinson, D. J. Cavalieri, and P. Gloersen (2002), Variability of Antarctic sea ice 1979-1998, *J. Geophys. Res.*, *107*(C5), 21 pp., 10.1029/2000JC000733.

Figure Captions

Figure 1. Location maps for the north and south polar regions.

Figure 2. Areal distributions of Northern and Southern Hemisphere March and September sea ice covers, averaged over 1979-2004, as observed from satellite data (A) and as simulated by each of 11 major GCMs (B-L). In each case the late summer sea ice distribution (September in the Northern Hemisphere, March in the Southern Hemisphere) is depicted in dark shading and the late winter sea ice distribution (March in the Northern Hemisphere, September in the Southern Hemisphere) extends over both the dark and light shaded regions.

Figure 3. Annual cycle of monthly sea ice extents, averaged over 1979-2004, as observed from satellite data (A) and as simulated by each of 11 major GCMs (B-L), for the Northern (thickest curves) and Southern (thinner curves) Hemispheres. The observed results (A) are repeated on each of the other plots, as dotted curves, for comparison purposes. Vertical bars show the standard deviations of the monthly mean ice extents.

Figure 4. Difference between the modeled 1979-2004 monthly average sea ice extents and the satellite-based observations (modeled – observed), for each of 11 major GCMs, for both the Northern (A) and Southern (B) Hemispheres.

Figure 5. Annual cycle of monthly sea ice extents, averaged over 1979-2004, from satellite data (dashed curves) and from the averaged results from 11 major GCMs (solid curves), for the Northern (thickest curves) and Southern (thinner curves) Hemispheres.

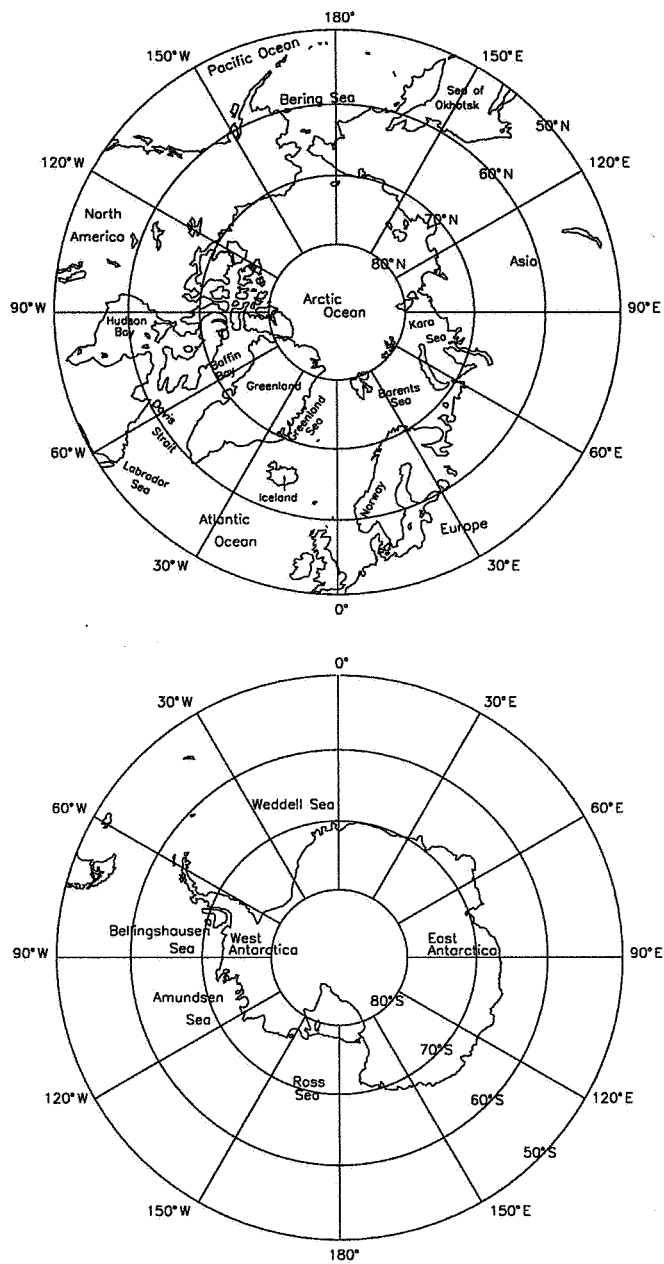


Figure 1. Location maps for the north and south polar regions.

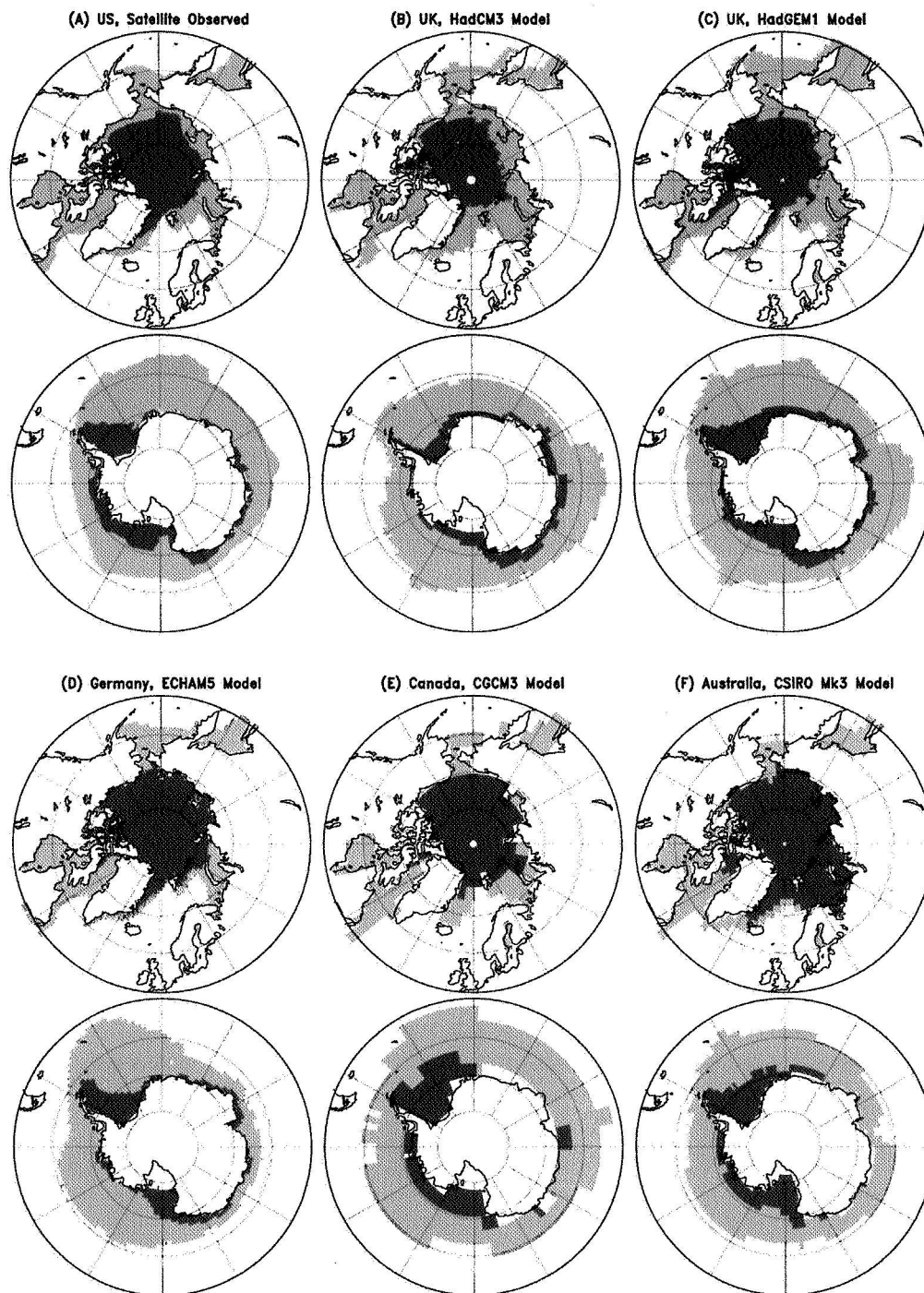


Figure 2 (first of two pages). Areal distributions of Northern and Southern Hemisphere March and September sea ice covers, averaged over 1979-2004, as observed from satellite data (A) and as simulated by each of 11 major GCMs (B-L). In each case the late summer sea ice distribution (September in the Northern Hemisphere, March in the Southern Hemisphere) is depicted in dark shading and the late winter sea ice distribution (March in the Northern Hemisphere, September in the Southern Hemisphere) extends over both the dark and light shaded regions.

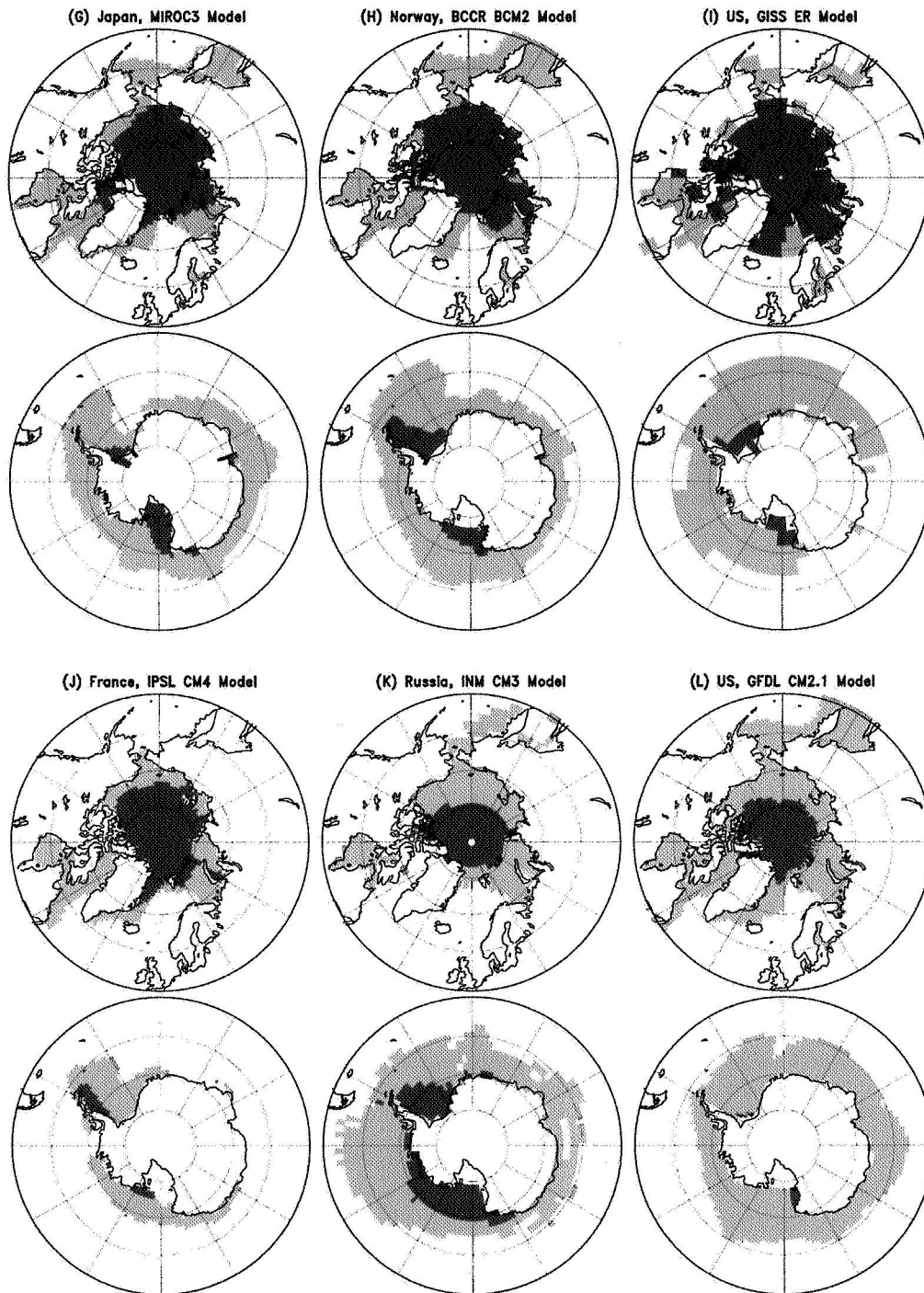


Figure 2 (continued). Areal distributions of Northern and Southern Hemisphere March and September sea ice covers, averaged over 1979-2004, as observed from satellite data (A) and as simulated by each of 11 major GCMs (B-L). In each case the late summer sea ice distribution (September in the Northern Hemisphere, March in the Southern Hemisphere) is depicted in dark shading and the late winter sea ice distribution (March in the Northern Hemisphere, September in the Southern Hemisphere) extends over both the dark and light shaded regions.

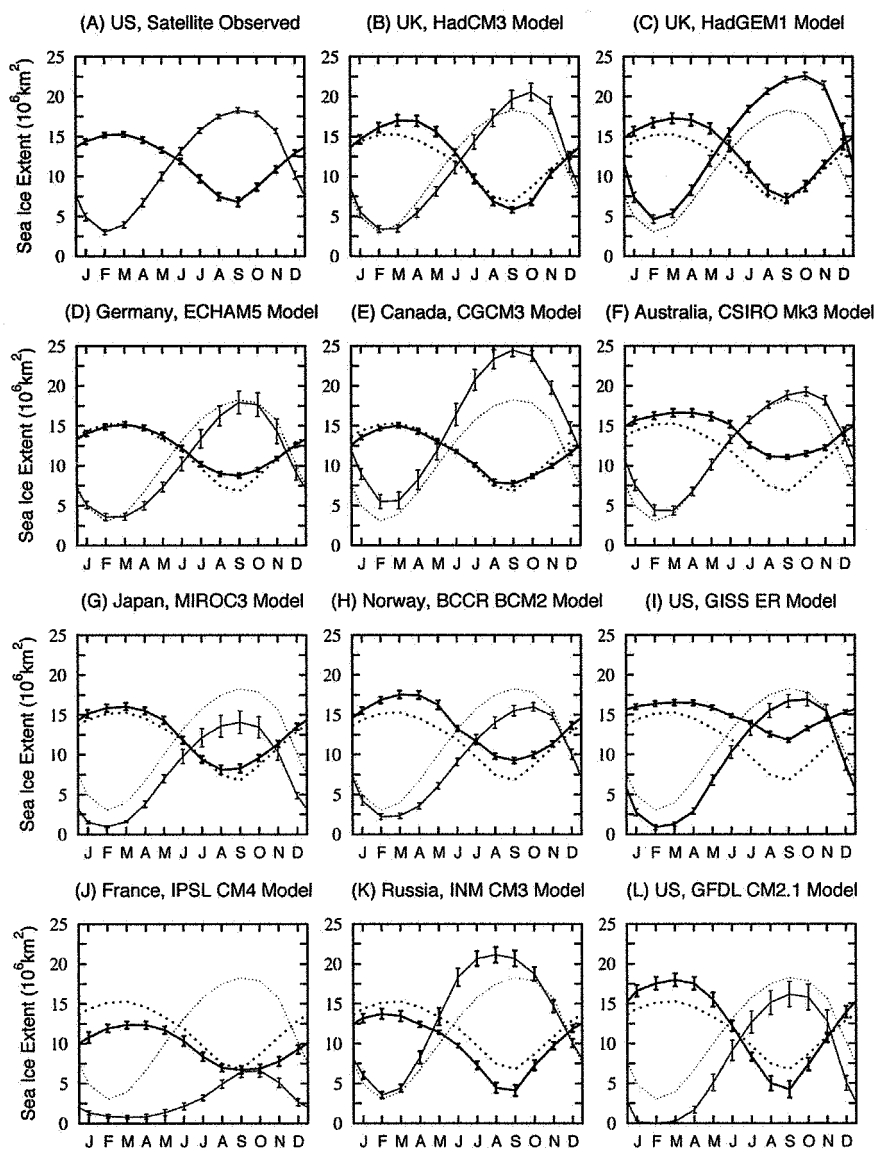


Figure 3. Annual cycle of monthly sea ice extents, averaged over 1979-2004, as observed from satellite data (A) and as simulated by each of 11 major GCMs (B-L), for the Northern (thickest curves) and Southern (thinner curves) Hemispheres. The observed results (A) are repeated on each of the other plots, as dotted curves, for comparison purposes. Vertical bars show the standard deviations of the monthly mean ice extents.

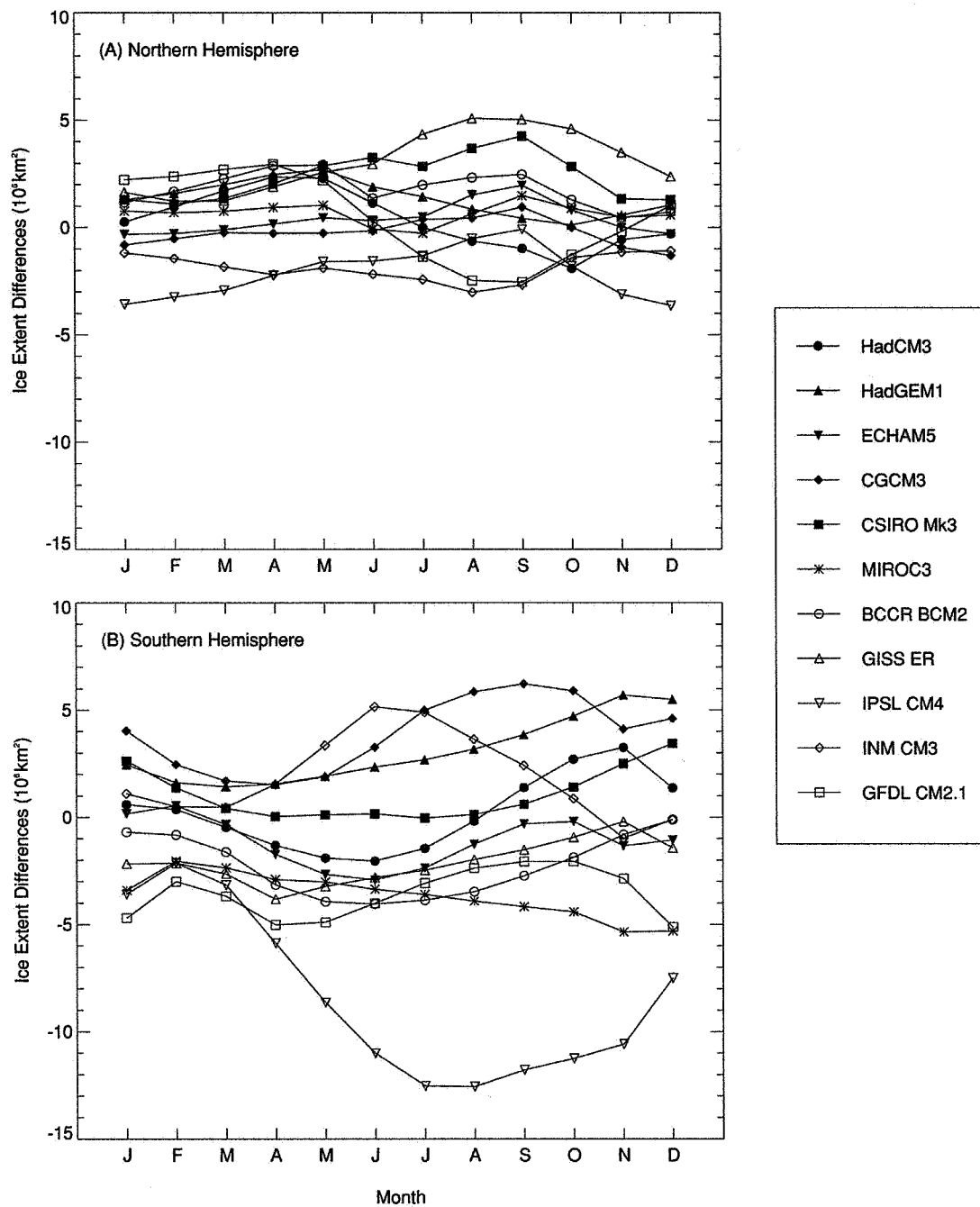


Figure 4. Difference between the modeled 1979-2004 monthly average sea ice extents and the satellite-based observations (modeled – observed), for each of 11 major GCMs, for both the Northern (A) and Southern (B) Hemispheres.

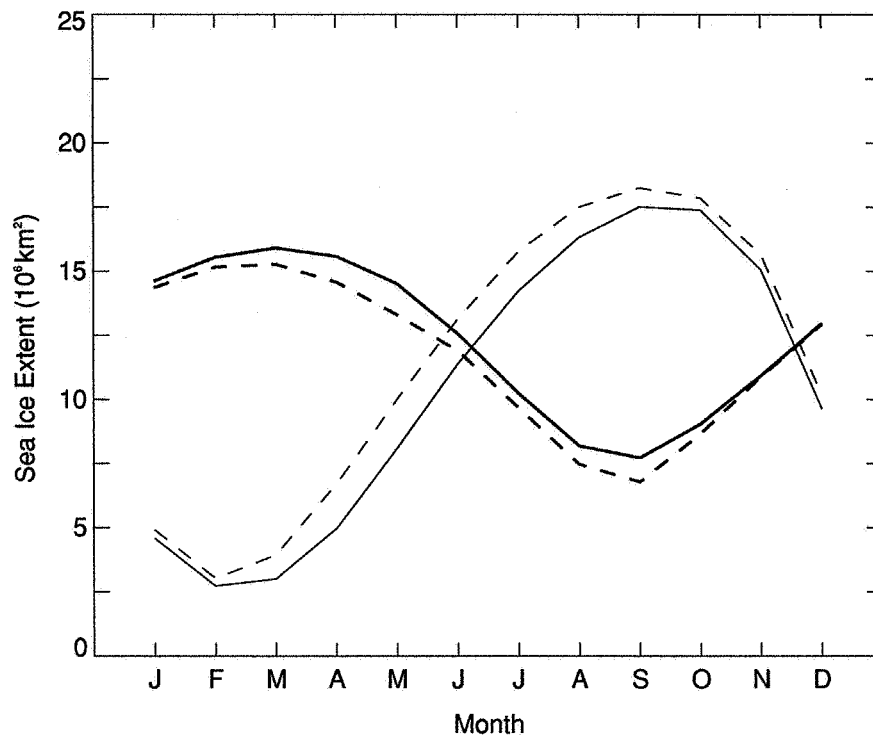


Figure 5. Annual cycle of monthly sea ice extents, averaged over 1979-2004, from satellite data (dashed curves) and from the averaged results from 11 major GCMs (solid curves), for the Northern (thickest curves) and Southern (thinner curves) Hemispheres.

Evaluation of the Simulation of Arctic and Antarctic Sea Ice Coverages
by Eleven Major Global Climate Models

Claire L. Parkinson¹, Konstantin Y. Vinnikov², and Donald J. Cavalieri¹

¹NASA Goddard Space Flight Center, Greenbelt, MD 20771

²University of Maryland, College Park, MD 20742

Abstract

Comparison of polar sea ice results from 11 major global climate models and satellite-derived observations for 1979-2004 reveals that each of the models is simulating seasonal cycles that are phased at least approximately correctly in both hemispheres. Each is also simulating various key aspects of the observed ice cover distributions, such as winter ice not only throughout the central Arctic basin but also throughout Hudson Bay, despite its relatively low latitudes. However, some of the models simulate too much ice, others too little ice (in some cases varying depending on hemisphere and/or season), and some match the observations better in one season versus another. Several models do noticeably better in the Northern Hemisphere than in the Southern Hemisphere, and one does noticeably better in the Southern Hemisphere. In the Northern Hemisphere all simulate monthly average ice extents to within $\pm 5.1 \times 10^6 \text{ km}^2$ of the observed ice extent throughout the year; and in the Southern Hemisphere all except one simulate the monthly averages to within $\pm 6.3 \times 10^6 \text{ km}^2$ of the observed values. All the models properly simulate a lack of winter ice to the west of Norway; however, most do not obtain as much absence of ice immediately north of Norway as the observations show, suggesting an under simulation of the North Atlantic Current. The spread in monthly averaged ice extents amongst the 11 model simulations is greater in the Southern Hemisphere than in the Northern Hemisphere and greatest in the Southern Hemisphere winter and spring.

paper for submission to the *Journal of Geophysical Research*, November 2005

Corresponding author: Claire L. Parkinson (claire.l.parkinson@nasa.gov; 301-614-5715).

Evaluation of the Simulation of Arctic and Antarctic Sea Ice Coverages
by Eleven Major Global Climate Models

Claire L. Parkinson¹, Konstantin Y. Vinnikov², and Donald J. Cavalieri¹

¹NASA Goddard Space Flight Center, Greenbelt, MD 20771

²University of Maryland, College Park, MD 20742

Popular Summary

Global climate models (GCMs) are widely used to make projections about future climate conditions in the twenty-first century and beyond. For these projections to be reliable, it is important that each element of the climate is being properly simulated. In this paper, we examine how well 11 major GCMs are doing in the simulation of polar sea ice, by comparing the sea ice simulations averaged for the years 1979-2004 with satellite observations over the same time period. Sea ice is important because it spreads over vast regions and has various impacts on the polar climate and ecology, such as restricting exchanges between the atmosphere and ocean, and reflecting solar radiation back toward outer space. The results show that there are many differences among the simulations from the different models. Some of the models do better in simulating the ice in the Arctic, others do better in simulating the ice in the Antarctic. Some simulate too much ice, while others simulate too little ice. However, each of the models properly simulates some of the basic features of the ice covers, such as significantly more ice in the winter than the summer (in each hemisphere) and winter ice not only throughout the central Arctic basin but throughout Hudson Bay, which is at much lower latitudes. They all also properly simulate the absence of ice for a substantial distance to the west of Norway, an area that is at higher latitudes than Hudson Bay but is warmed by ocean currents from the south. Still, the models do not obtain as much absence of ice immediately north of Norway as the observations show, suggesting that they are not simulating a strong enough North Atlantic Current. Also, some of the simulations show much more significant deficiencies, including one that simulates an Antarctic ice cover that is less than a third as extensive as the observed ice cover. All of the simulations have at least minor deficiencies, and these are likely to have impacts on the model predictions regarding future polar climates. The hope is that this work, by identifying strengths and weaknesses of the sea ice simulations, will help modeling groups in focusing on particular areas needing improvement.

paper for submission to the *Journal of Geophysical Research*, November 2005

Corresponding author: Claire L. Parkinson (claire.l.parkinson@nasa.gov; 301-614-5715).